This article has been published in: Clin Oral Investig. 2017 Dec;21(9):2695-2707.

Authors:

Raquel Osorio[1].
Camilo Andrés Alfonso-Rodríguez[2].
Estrella Osorio[1].
Antonio L. Medina-Castillo[3].
Miguel Alaminos[2].
Manuel Toledano-Osorio[1].
Manuel Toledano[1].

Affiliations and addresses:
1. Dental School. University of Granada. Colegio Máximo, Campus de Cartuja s/n. 18017 Granada, Spain. Research Institute IBS.

2. Tissue Engineering Group, Department of Histology, University of Granada, 18012, Granada, Spain. Research Institute IBS.

3. NanoMyP. Spin-Off Enterprise from University of Granada. Edificio BIC-Granada. Av. Innovación 1. 18016 Armilla, Granada, Spain.

Title:
Novel Potential Scaffold for Periodontal Tissue Engineering

Corresponding author:
Raquel Osorio
Dental School, University of Granada.
Colegio Máximo, Campus de Cartuja s/n 18017 Granada, Spain.
Phone: +34-958243793; Fax: +34-958240908.
E-mail: rosorio@ugr.es

CONFLICT OF INTERESTS: None. The authors declare no conflict of interests.

Abstract:

Objective: Characterization of novel calcium and zinc loaded electrospun matrices for periodontal regeneration. Materials and Methods: A polymethylmetacrylate-based membrane was calcium or zinc loaded. Matrices were characterized morphologically by atomic force and scanning electron microscopy, and mechanically probed by a nanoindenter. Biomimetic calcium phosphate precipitation on polymeric tissues was assessed. Cell viability tests were performed using oral mucosa fibroblasts. Data were analyzed by Kruskal-Wallis and Mann-Whitney tests or by ANOVA and Student-Newman-Keuls multiple comparisons. Results: Zinc and calcium loading on matrices did not modify their morphology but increased nanomechanical properties and decreased nanoroughness. Precipitation of calcium and phosphate on the matrices surfaces was observed in zinc-loaded specimens. Matrices were found to be non-toxic to cells in all the assays. Calcium and zinc-loaded scaffolds presented a very low cytotoxic effect. Conclusions: Zinc-loaded membranes permit cells viability and promoted mineral precipitation in physiological conditions. Based on the tested nanomechanical properties and scaffold architecture, the proposed membranes may be suitable for cell proliferation. Clinical Relevance: The ability of zinc-loaded matrices to promote precipitation of calcium phosphate deposits, together with their observed non-toxicity and its surface chemistry allowing covalent binding of proteins, may offer new strategies for periodontal regeneration.

Keywords: regeneration, calcium, zinc, nanopolymers, scaffolds

1. Introduction

Bone-ligament periodontal complex regeneration has, in many cases, an unpredictable clinical outcome and remains a challenge in Dentistry. The use of reabsorbable tissue-engineered matrices to induce bone formation, when additional support is needed, is not always successful. A major limitation is the inability to exert spatiotemporal control over the wound-healing process [1]. Most of the employed reabsorbable membranes (e.g. collagen, polylactide-co-glycolide, polycaprolactone) and bone graft substitutes (e.g. hydroxyapatite -HAp- and other calcium phosphates) show a relatively fast rate of biodegradation. It should be taken into account that the healing period of the alveolar bone, after periodontal regeneration or after extraction usually needs 6 to 12 months. Currently, employed reabsorbable materials may be disadvantageous, as dissolution behaviors are not as long-lasting as required [2]. Moreover, some degradation products from these reabsorbable materials have low pH, they may not be cytocompatible [1,2] and could also alter the remineralization processes [1].

Even when much research is being conducted about reabsorbable periodontal membranes, polytetrafluoroethylene (PTFE), a non-reabsorbable synthetic polymer, still represent the gold-standard for clinicians, due to its higher predictability if compared to reabsorbable membranes [3]. However, PTFE possess important disadvantages as: low adhesiveness for cells, total absence of the capability of connecting to the bone tissue and providing osseointegration, without formation of a connective tissue interlayer and lack of antibacterial properties [3].

A successful matrix for bone regeneration should resemble the morphology of natural bone. Natural bone is a hybrid of inorganic-organic tissue composed of hydroxyapatite nanocrystals and collagen fibers (with diameters ranging from 50 to 500 nm) assembled into a porous mesh, with interconnected pores [4]. Bone is nanostructured, so nanosized materials should be the best choice for bone substitutes. The advantages of these nanomaterials reside in their high porosity, and high surface area-to-volume ratio that will enhance the adsorption of proteins (*i.e.*, fibronectin, vitronectin, laminin and collagen), which will mediate cell-surface interactions [5].

New nanostructured polymer membranes based on polymethylmethacrylate are proposed. Polymethylmethacrylates (PMMA) are non-reabsorbable but biocompatible polymers, which have been widely used to clinically fix prostheses to bone or for vertebroplasty, intraocular lenses, orthopaedic bone cements, skull defects reparation or mandibular reconstruction between others, due to its excellent tissue compatibility [6,7]. Presented polymeric solution may be spun. In the electrospinning process, randomly distributed nanofibers are created. Polymeric nanofibers are suitable scaffolds for tissue engineering applications. Electrospinning represents a reliable method to fabricate long continuous strands of nanofibers with a diameter ranging from 50 to 1,000 nm. Electrospun nanofibers possess the advantages of a very high surface-to-volume ratio and pore sizes ranging from several to tens of micrometers [5].

PMMA shows weak interactivity against tissue cells, and promotes the formation of fibrotic tissue [7]. To enhance tissue-biomaterial interaction, and therefore tissue integration, strategies such as modification of surface properties have been previously employed. Chemical surface modification has been proposed to improve surface properties. It can be obtained through the addition of functional chemical groups or

bioactive ions. Improved osteogenic ability [8] and increased osteoconductivity [9] have been associated with the use of calcium and zinc containing bioactive materials. These ions may also help to overcome chronic infections, as calcium and zinc have been demonstrated to possess significant antimicrobial activities [10,11]. Therefore, zinc and calcium were added into our polymer matrices.

The aim of the study is the design and characterization of a novel bioactive and cytocompatible nanostructured membranes loaded with calcium or zinc for periodontal and bone regeneration.

2. Materials and methods

2.1. Preparation of artificial tissues

Nanostructurated membranes were acquired from NanoMyP (Granada, Spain). They were fabricated through electrospinning, with a commercial polymeric blend (PolymBlend®). Their surfaces were then modified by chemical functionalization. PolymBlend® is composed of a mixture of two high molecular weight copolymers: methyl methacrylate-co-hydroxyethyl methacrylate (average Mw 200 kDa, PDI<2.5), and methyl acrylate-co-hydroxyethyl acrylate (average Mw 2,000 kDa, PDI<1.5). The percentage of the hydroxylated monomers in the polymer blend depends on the ratio in which the two copolymers are mixed. The recommended ratio for processing by electrospinning is 1:1, which corresponds to 41% of hydroxylated monomers. PolymBlend® has been thoroughly optimized for the production by electrospinning of non-woven nanofiber mats with adequate mechanical and physicochemical properties such as high resistance to abrasion, high tensile strength, high bursting resistance, adequate flexibility and elasticity, easy handling, high resistance to acids and bases, and temperature resistance. Membranes were loaded with calcium or zinc, and incubated at room temperature for 3 days. They underwent continuous shaking in different aqueous solutions of $ZnCl_2$ or $CaCl_2$ (containing zinc or calcium at 40 ppm) (pH:6.5), in order to reach the adsorption equilibrium of metal ions. Then, the suspensions were centrifuged (60 min, 12,000 rpm, two cycles) and the matrices were separated from the supernatant. For the surface preactivation, the OH-Matrix, Zn-Matrix and Ca-Matrix surfaces were reacted with a sodium carbonate buffer solution (333 mM; pH=12.5) for 2 h and gently washed with water. Thus, due to the partial hydrolysis of ester bonds, carboxyl groups were disposed on their surfaces [7].

2.2. Atomic force microscopy (AFM) and Field emission scanning electron microscopy (FESEM) *surface characterization*

The imaging process was undertaken in the tapping mode, using an AFM (Nanoscope V, Digital Instruments, Veeco Metrology group, Santa Barbara, CA, USA) with a calibrated vertical-engaged piezo-scanner. A 10-nm-radius silicon nitride tip was attached to the end of an oscillating cantilever that came into intermittent contact with the surface at the lowest point of the oscillation. Changes in vertical position of the AFM tip at resonance frequencies near 330 kHz provided the height of the images registered as bright and dark regions. Three 20 x 20 μm digital images were recorded from each surface, with a slow scan rate (0.1 Hz). Measurements were performed in a wet cell, under hydrated conditions. For each image, five randomized boxes (5 μm × 5 μm) were created to examine surface nanoroughness (SRa, in nanometer). Fiber diameters and fiber to fiber distances ranges were also measured using a specific software (Nanoscope Software version V7). For fiber diameters, measurements were corrected for tip broadening by the equation $e = 2r$, where e is the error in the horizontal

dimension and *r* is the tip's radius [12]. ANOVA and Student-Newman-Keuls multiple comparisons were performed ($p<0.05$).
Additional surface characterization was performed by FESEM (GEMINI, Carl Zeiss SMT, Germany) at 2.5 Kv, 3.5 mm working distance. Microscope was attached to an energy dispersive analysis system (EDX). Elemental analysis was performed at a working distance of 15 mm (Inca 300 and 350, Oxford Instruments, Oxford, UK).

2.3. Acellular static in vitro bioactivity test
Matrices were soaked in 20 ml of simulated body fluid solution (SBFS) [pH 7.45] in sterile flasks for 7 days [13,14]. Reagents per 1000 ml of SBFS were: 8.035 g of NaCl, 0.355 g of $NaHCO_3$, 0.225 g of KCl, 0.231 g of $K_2HPO_4 \cdot 3H_2O$, 0.311 g of $MgCl_2 \cdot 6H_2O$, 39 g of 1M HCl,0.292 g of $CaCl_2$, 0.072 g of Na_2SO_4, 118 g of Tris, 0 to 5 ml of 1M HCl for final pH adjustment. After drying, surfaces were analyzed by FESEM at 2.5 Kv, 3.5 mm working distance and elemental analysis was done by means of an EDX attached to the FESEM, at a working distance of 15 mm.

2.4. Nanomechanical properties assessment
Nanomechanical properties mappings were conducted using a Hysitron Ti Premier nanoindenter (Hysitron, Inc., Minneapolis, MN) equipped with nano-DMA III, a commercial nano-DMA software. Modulus mapping of the samples was conducted by imposing a quasistatic force setpoint, F_q=2 μN, to which a sinusoidal force of amplitude F_A=0.10 μN and frequency *f*=200 Hz was superimposed. The resulting displacement (deformation) at the site of indentation was monitored as a function of time. Data from regions approximately 20×20 μm in size were collected using a scanning frequency of 0.2 Hz. Specimens were scanned under a hydrated condition.

Under steady conditions (application of a quasistatic force) the indentation modulus of the tested sample, *E*, can be obtained by application of different models that relate the indentation force, *F*, and depth, *D* [15]. Most of these theories assume proportionality between the force and the indentation modulus:

equation (1)

$$F = g(D)E \Rightarrow E = \frac{F}{g(D)}.$$

where, *g* (*D*) is a function on the indentation depth, which depends on the geometry of the probe of the indenter. For example, for a spherical probe, the Hertzian contact theory predicts [15]:

equation (2)

$$g(D) = \frac{4R^{1/2}D^{3/2}}{3\left(1-\nu^2\right)}.$$

In this equation *R* is the radius of the spherical probe and ν is Poisson′s ratio of the tested sample.
As mentioned above, in nano-DMA experiments an oscillatory force is superimposed to a quasistatic force:

equation (3)

$$F = F_q + F_A \sin\left(2\pi ft\right),$$

with t being the time. Under this imposed force, the indentation depth takes the following form:

equation (4)

$$D = D_q + D_A \sin\left(2\pi ft - \delta\right).$$

This means that the indentation depth also oscillates around a quasistatic value, with the same frequency that the oscillating force and delayed by a phase lag δ. In the limit of $FA<<Fq$ we can expand Eq. (1) to a first order Taylor approximation, to obtain:

equation (5)

$$F_q + F_A \sin\left(2\pi ft\right) = g(D_q)E + g'(D_q)\left|E^*\right|D_A \sin\left(2\pi ft - \delta\right).$$

In this equation, g' is the first derivative of g, and E^* is the complex dynamic indentation modulus. Now, the time-dependent terms can equaled and changed the time origin, to write:

equation (6)

$$F_A \sin\left(2\pi ft + \delta\right) = g'(D_q)\left|E^*\right|D_A \sin\left(2\pi ft\right).$$

Now, the oscillating force may be decomposed into two terms, the in-phase term, F′, and the out-of-phase term, F″ [16]:

equation (7)

$$F_A \sin\left(2\pi ft + \delta\right) = F_A \cos\delta \sin\left(2\pi ft\right) + F_A \sin\delta \cos\left(2\pi ft\right) =$$
$$= F_A' \sin\left(2\pi ft\right) + F_A'' \cos\left(2\pi ft\right) = F' + F''$$

Then, from this decomposition two dynamics moduli can be extracted:

equation (8)

$$E' = \left|E^*\right|\cos\delta = \frac{F_A \cos\delta}{g'(D_q)D_A} = \frac{F_A'}{g'(D_q)D_A},$$

which is the in-phase or storage (elastic) modulus.

equation (9)

$$E'' = |E^*| \sin\delta = \frac{F_A \sin\delta}{g'(D_q) D_A} = \frac{F_A''}{g'(D_q) D_A},$$

which is the out-of-phase or loss (viscous) modulus. Note the position of the phase lag, δ, in these equations.

These coefficients are directly related with measured parameters, without any particular assumption, except the consideration of the system consisting of the sample and the instrument tip as a driven simple oscillator under stationary conditions.

Obtained data were submitted to ANOVA and Student-Newman-Keuls multiple comparisons ($p<0.05$).

2.5. Cell viability analysis

Establishment of primary cultures of oral mucosa fibroblasts was performed. Ten normal human oral mucosa biopsies with an average volume of 8 mm^3 were obtained from healthy donors at the School of Dentistry of the University of Granada. Written informed consent was always obtained and the research protocol was approved by the Institutional Review Board. To obtain primary cultures of human oral mucosa fibroblasts, tissues were enzymatically de-epithelized and the lamina propria was digested in a mixture of Dulbecco's Modified Eagle's Medium (DMEM) and 2 mg/mL *Clostridium histolyticum* collagenase I (Gibco BRL Life Technologies, Karlsruhe, Germany). Detached fibroblasts were collected by centrifugation and expanded in culture flasks containing DMEM supplemented with 10% fetal calf serum (FCS) and 1% antibiotic-antimycotics solution (final concentration 100 U/mL penicillin G, 0.10 mg/mL streptomycin and 0.25 µg/mL amphotericin B) (all from Sigma-Aldrich, Steinheim, Germany). Cells were incubated at 37°C in 5% carbon dioxide under standard culture conditions. The medium was changed every 3 days, and the cells were subcultured in a solution of 0.5 g/L trypsin and 0.2 g/L EDTA at 37°C for 10 min. For all experiments, cells from the first three passages of these human oral mucosa fibroblast cell cultures were used [17].

Fourteen study groups were analyzed in this work: 0.2, 0.4, 2 or 4 mg of OH-Matrix, Zn-Matrix and Ca-Matrix, positive controls -cells cultured in DMEM without matrices- and negative controls -cells treated with 2 % triton X-100 (Sigma, St. Louis, MO)-. Triton X-100 is a chemical compound that has been previously described to produce high cytotoxic effects. In all cases, cells were analyzed after 24 h of exposition of the cells to each culture condition [17].

Cell viability was evaluated by three different techniques:

1) Cell death, as determined by nuclear membrane integrity, was assessed by quantifying the liberated deoxyribonucleic acid (DNA) to the culture media. Supernatants of each sample were obtained, and 10-µL aliquots were diluted ten times in distilled water free of nuclease (Ambion-Life Technologies, Austin, TX, USA). The DNA, in the medium, was quantified spectrophotometrically (SmartSpec Plus, Bio-Rad, Hercules, CA, USA) at wavelengths in the range of 260–280 nm. The mean values and standard deviations of three independent experiments are reported here for each experimental group.

2) The LDH assay (Roche, Germany) detects the amount of lactate dehydrogenase (LDH), enzyme released by cells with damaged membranes as indicator of cell death. Cells were incubated with previously prepared particles dilutions, and LDH was quantified in the supernatant corresponding to each experimental group. In order to investigate particle interferences with the measurement, cell supernatants were transferred after centrifugation (10 min, 200g) in a new 96-well plate, and LDH assay was performed. For each experimental group, five independent determinations were taken.

3) By examining the cytoplasmic esterase function and cell membrane integrity with a fluorescence-based method using the Live/Dead commercial kit (Life Technologies, Carlsbad, CA, USA). This method uses calcein-AM, which is metabolically modified by living cells to a green pigment, and ethidium homodimer-1, which stains the nuclei of dead cells in red. After incubation of the cells with each biomaterial, the supernatants were discarded and cells were washed with PBS, incubated with the Live/Dead solution for 15 min as indicated by the manufacturer, and washed with PBS. Samples were then observed by fluorescence microscope (Nikon Eclipse 90i, Nikon, Japan). For each experimental condition, five images were taken. The images were processed with *Image J* software (MacBiophotonics, Ontario, Canada) developed at McMaster University, in order to quantify the number of red (dead) and green (live) cells. For each condition, five independent determinations were taken and an average of 1,000 cells was analyzed.

Normalized average and standard deviation results were calculated by considering the results obtained for the positive controls as 0% mortality (100% survival) and those attained for the negative controls as 100% mortality (0% survival).

The Kruskal-Wallis and the Mann-Whitney tests were used. Statistical significance was set at $p<0.05$.

3. Results

3.1. AFM and FESEM matrices characterization

AFM images of the three different matrices are shown in Figure 1. Overlapped and randomly distributed nanofibers, as a result of the electrospinning manufacturing process, may be observed. Fiber sizes, fiber to fiber distances and surface roughness are displayed in table 1. Mean and standard deviation (SD) of nanofiber sizes, in nm, range from 302.40 (SD 19.13) to 312.72 (SD 28.66); and no differences were found between groups (P=0.25). These nanofibers appeared grouped in microfibers with similar mean sizes ranging from 2.05 (SD 0.30) to 1.97 (SD 0.18) nm (P=0.29). As fibers are randomly distributed, fiber to fiber distances were in a wide range, between 110 nm to 11.5 microns. Significant differences ($p<0.001$) were found between mean surface roughness (SRa) of OH-Matrix [137.07 (SD 21.84) nm], Zn-Matrix [108.40 (SD 16.17) nm] and Ca-Matrix [82.74 (SD 19.64) nm]. FESEM images of matrices are presented in figures 2a to 2c. The fiber size was approximately 300 nm in diameter. Morphology and random distribution of fibers, which may be observed, were not altered by calcium or zinc loading onto electrospun fiber matrices.

3.2. Acellular static in vitro bioactivity test

FESEM images of matrices before and after 7 days of immersion are presented in figure 2. After immersion, differences between groups were evidenced. At OH-matrices some

rounded deposits were observed rarely on the samples. Traces of calcium were found at the EDX spectra (Figures 2d, 2e and Ep1). On Ca-matrices, an increase in nanofiber diameter was found, and nanofiber lost their smooth appearance. Spotty calcium deposits were uniformly distributed throughout nanofibers surfaces. Calcium was also identified after EDX analysis (Figures 2f, 2g and Ep2). On Zn-matrices samples, nanofiber diameter was highly increased (from 300 to about 500 nm). Fibers lost the smooth appearance of their surface. Nanodeposits of mineral (100 nm) were randomly distributed onto the nanofibers surfaces. Calcium and phosphorous were encountered at the EDX spectra on nanofibers surfaces (Figure 2h and Ep3). Numerous agglomerations of other spherical nanocrystals (bigger than 200 nm) were identified onto the Zn-Matrix surface. Calcium, phosphorous and zinc were encountered after elemental analysis of these crystal agglomerations (Figure 2i and Ep4). At the presented EDX spectra, chloride and sodium were detected after SBFS immersion; magnesium is a contaminant element from the sample holder.

3.3. Nanomechanical properties assessment

Means and standard deviations of complex, loss and storage modulus are displayed in table 2. Zn-matrices achieved the highest elastic or storage modulus followed by Ca-matrices. OH-matrices exhibit the lowest [mean and SD in GPa attained for each group respectively were: 17.40 (5.36) > 13.31 (3.18) > 10.03 (4.46)]. Same trend and significance was observed for loss and storage modulus. Tan delta values were lower for Ca-Matrix [Mean 0.63 (SD 0.14)] and Zn-matrix [Mean 0.65 (SD 0.15)] without differences between them. OH-Matrix attained the highest value [Mean 1.07 (SD 0.52)]. Images from NanoDMA analyses in scanning mode for the tested matrices are presented in figure 3.

3.4. Cytotoxicity tests

Results from cytotoxicity assays are shown in figure 4. For the three employed techniques, all the experimental groups were significantly different from both controls. Liberated DNA to the culture media was found to be under 5% -if normalized with the control groups- for all types of tissues and weights (Figure 4a). According to LDH enzyme quantification in the culture medium, normalized values were about 25%, and always under 30%, and resulted similar independently of the tissue type or weight (Figure 4b). And finally, after examining the integrity of the cytoplasmic esterase function and cell membrane integrity with a fluorescence-based method (Live/Dead), human fibroblasts viability stated above 90% in the non-loaded scaffolds, and above 80% in calcium and zinc-loaded groups. All the experimental groups attained cell viability, significantly different from controls. Between tested materials, small differences existed as Ca-matrices were more cytotoxic than Zn-matrices ($P<0.02$) and both Ca and Zn-matrices resulted to be less cytocompatible than OH-matrices ($P<0.005$ and $p<0.02$ respectively) (Figure 4c). Representative fluorescence microscopy images for each experimental group are presented in Figure 5. After analyze the cytotoxic cell damage induced by the three experimental tissues, it may be stated that they produced a negligible degree of cytotoxicity (Figure 4 and 5). Thus, a dose-dependent effect was not noticed in any of the studied groups and applied tests.

4. Discussion.

New nanostructured polymer membranes based on polymethylmethacrylate are proposed to be used for guided bone regeneration in periodontal applications. The membranes are comprised of a series of non-woven nanofibres produced by electrospinning technology. Biomaterials should be designed and characterized based on application needs. There are an impressive number of suitable methods for scaffolds characterization. Selecting appropriate methods is challenging as not all methods will be relevant in every case. For the presented membranes a multi-parameter characterization is necessary: surface characterization (porosity, pore size and roughness), mechanical surface properties, static in vitro bioactivity and biological characterization by cell culture methods are required [18,19]. AFM and a dynamic nanoindenter were selected as they have become essential tools permitting to measure accurately on the nanoscale, producing high resolution images and requiring little or no sample preparation. The *in vitro* bioactivity of a material is defined by its capacity to form bone-bonding with host bone and it can be predicted from the calcium phosphate (Ca/P) deposit formation on its surface, after SBFS immersion [13]. Biological characterization was performed by combining three different cell culture experimental techniques: cytoplasmic (LDH) and nuclear (DNA) membrane integrity assays, and the LIVE/DEAD cytoplasmic esterase function and cell membrane integrity [17]. A more detailed *in vitro* cell culture assays to establish if late bone markers are observed, space-making ability at the implantation site and cell-occlusiveness are also important points that will be performed in the future, this research will require relevant experimental animal models for analysis [19].

Calcium and zinc complexing on polymeric tissues did not modify their morphology (Figures 1, 2a, 2b and 2c), but increased mechanical properties and decreased nanoroughness (Tables 1 and 2). Scaffold architecture greatly influences cell attachment and migration and it is a fundamental part of tissues analysis [20]. Attained differences in nanoroughness were encountered between the three analyzed tissues, ranging from 82.74 to 137.07 nm. These differences may not be crucial in respect to cell behavior. It has been reported that nanometric porosity ranging from 50 to 500 nm selectively enhances protein adsorption (including fibronectin and vitronectin) contributing to cell attachment [21]. Attained roughness values were within the previously reported cell-adhesion favorable range. Cells growing on membranes containing pores between 5 to 8 microns showed increased osteogenic differentiation [20]. These pores sizes are frequently encountered in the presented tissues, being approximately 30% of pores on each tissue. The nanofiber diameter of tested matrices is around 300 nm, which is also favorable for cell attachment. Mimicking collagen nanofibers diameters have been shown to enhance cell attachment on tissues about 1.7 fold [21]. Even when specific studies of cell adhesion and proliferation need to be conducted, the hydrophilicity of tested surfaces [22], and nanoroughness are important parameters that will promote protein non-specific adhesion and cellular attachment to proposed matrices [7,21].

To the best of our knowledge, this is the first study that reports on the dynamic nanomechanical properties of polymeric nanostructurated scaffolds for periodontal membranes. Polycaprolactone electrospun tissues have also been proposed as periodontal membranes [10,11]. The nanomechanical properties of individual electrospun polycaprolactone nanofibers were previously reported, concluding, that mechanical properties of these nanofibers are high below those of other proteins as collagen or fibrinogen electrospun nanofibers [23]. However, measuring properties of individual nanofibers is not completely reliable as it does not relate to the clinical use of these materials. These measurements performed on an individual fiber do not take into account the force dissipation due to molecular interactions within the fibers of the network, and the force dissipation *via* interstitial spaces and flows [24]. It is difficult to establish comparisons, due to the lack of studies. Tested matrices achieved significantly different dynamic storage modulus following the trend: OH-matrix 6.29 GPa (SD: 2.58) < Ca-matrix 10.23 GPa (SD: 3.03) < Zn-matrix 13.29 GPa (SD: 5.25) (Table 2, Figure 3). Storage moduli of Zn-matrices are within the range of the nanoindentation moduli of calcified trabecular bone, which is about 15 GPa [25]. These values highly differ from the storage modulus calculated for highly cross-linked collagen scaffolds, which are around 1GPa [26]. The importance of these results is supported by a recent finding stating that substrate stiffness can modify cell behavior, and cells may probe and respond to mechanics in fibrillar matrices [27].

Scaffolds have to perform under mechanical stress. Thereby, being able to control and tailor the structural-functional integrity becomes crucial [3]. Most of the recently proposed materials have poor mechanical properties compared to the native tissues that they are targeted to mimic or repair. Collagen fibrils, even when strengthened by covalent crosslinks [26], or polycaprolactone [28] are clear examples. Zn-matrices achieved the highest elastic or storage modulus (Mean 17.40 GPa -SD 5.36-) when compared with the rest of the groups (Table 2, Figure 3). They presented the highest ability to store potential energy which is released after deformation. Dissipation of energy within the structures is of prime importance in dynamic systems [29], such as the oral function, where oral structures require damping to absorb shock waves and alleviate stresses. Hence, improving damping characteristics becomes imperative for enhancing their robustness and forces resistance. During contact, low modulus materials lead to stress concentration resulting in transfer of energy (without dissipation) from the tissues to the adjacent structures. Hence, they may have adverse clinical implications. A general idea of the behavior of a viscoelastic material can be obtained by the value of the ratio represented by tan δ, with δ being the angle by which the displacement lags the force (Eq. 4). δ is a measure of the ratio of the energy dissipated by the system, to the energy stored in the system, that enables its elastic recoil. It reflects how well a material can get rid of the energy. The lower tan δ is, the greater the proportion of energy available in the system, for recoil [30]. Tan δ values higher than 1 represent liquid-like regions, contrarily to tan δ values smaller than 1, that represent gel-like behavior to solid-like behavior as tan δ approaches zero [31]. Ca- and Zn-matrices attained similar tan δ values (0.6) (Table 2, Figure 3), being more favorable to cells spreading as recently published by Baker et al. [27].

SBFS are fluids with ion concentrations nearly equal to those of human blood plasma and are employed for evaluating the bioactivity of biomaterials for hard tissue repair. Zinc deposition on tested tissues promoted biomimetic precipitation of Ca/P deposits and formation of HAp nanocrystals during SBFS immersion (Figure 2). The process of

Ca/P deposition may be explained as a surface phenomenom. Zinc complexation on tissues facilitated phosphate groups binding. These phosphate groups, at the surface, have under-coordinated oxygens, which lead to reactive surfaces that will attract calcium ions from SBFS [32]. This biomimetic deposition of Ca/P is considered as a coating method inspired by the natural process of biomineralization. Attained polymers/ceramics tissues represent a type of composite scaffold. They may be used as bone tissue substitutes, since they mimic to some extent the structure of natural bone extracellular matrix. Bioceramics are ineffective in terms of mechanical stability but they show osteoconductivity and bone-bonding ability. On the other hand, polymers are biocompatible and provide suitable mechanical properties [5]. Moreover, it should be considered that crystalline HAp is very slow to resorb, and most bone substitutes based on HAp do not resorb or resorb extremely slowly. However, if it precipitated HAp or nano-HAp it does so, facilitating hard tissue regeneration.

Biomimetic remineralization of the tested tissues will facilitate periodontal regeneration. HAp has been previously used not only for bone but also for periodontal regeneration. HAp facilitates formation of other bone apatite-like materials as carbonate HAp and it is able to stimulate cells, leading to the formation of bone. Moreover, HAp promotes osteoconductivity [33]. Osteoblasts, cementoblasts, periodontal ligament and pulp cells stimulated with extracellular Ca^{2+} and PO_4^{2-} increased bone morphogenetic protein-2 mRNA expression [2,34]. In periodontal ligament cells, fibroblast growth factor-2 (FGF-2) gene and protein expression levels are also augmented by increases in extracellular Ca^{2+} concentration [35]. FGF-2 promotes new bone formation, has a potent mitogenic effect on cementoblasts and periodontal ligament cells and enhances periodontal tissue regeneration. It also accompanied the formation of new bone and cementum with functionally oriented periodontal ligament fibers [35].

Data from the present study did not identify significant necrotic and/or apoptotic effects, of the tested tissues on human fibroblasts. Attained differences in results when comparisons are performed between various testing methods may, sometimes, difficult results interpretation. It reflects and highlights the importance of using a testing battery approach in cytotoxicity research [36]. If analyzed together, it is found that experimental groups differed greatly from the control. This suggests that tested tissues did not alter cell viability in any of the tested dosage (Figures 4 and 5), and are likely to be safe for use *in vivo*, in agreement with previous results [17,37]. PMMA has been previously shown to be non-cytotoxic [7]. Considering these outcomes, and assuming that dissolution of these tissues is unlikely, and unpolymerized monomers are absent, all toxicity observed will not be related to the matrices as such. It will be due to calcium or zinc ions on their surfaces.

Polycaprolactone membranes for periodontal regeneration have been previously loaded with zinc and calcium oxide nanoparticles. Displayed results stood that calcium-loading of polymeric membranes (less than 15 wt. % of CaO particles, relative to the total polymer weight) was not harmful to cells [11]. However, zinc oxide nanoparticles inclusion on the same polymers (5 to 30 wt % of ZnO nanoparticles, relative to the polymer weight) increased membranes cell cytotoxicity in a dose-dependent manner. It was obtained a reduction in cells viability up to 50% [10]. It may be concluded, that ionic zinc incorporation in the tissue did exert lower cytotoxicity than when zinc oxide nanoparticles are directly incorporated into the biomaterial.

Clear similarities have been described in proliferative potential and conditions between gingiva-derived and periodontal ligament-derived cells [38]. Hence, it should be stressed that just one single cell line was used, and it may not necessarily be extrapolated to other cell types.

Presented tissues seem to overcome the main disadvantages of the most used non-reabsorbable synthetic polymers in periodontal regeneration (PTFE membranes). They are: i) low adhesiveness for cells due to the high hydrophobicity, and ii) total absence of the capability of connecting to the bone tissue and providing osseointegration, without formation of a connective tissue interlayer [3]. Moreover, the use of metal ions, as antibacterial agents may also help, since they have demonstrated significant antimicrobial and antifungal activities [10,11]. The periodontal regeneration requires the use of appropriate scaffolds in a heavily contaminated oral environment [38,39]. It is also important to underscore that polymer-based scaffolds/membranes loaded with ZnO have been recently shown to display not only antibacterial properties [40], but also enhanced cell proliferation/wound healing [41]. However, based on the proven *in vitro* studies, future *in vivo* research using relevant animal models is needed to confirm the effectiveness of these matrices.

The main advantage of the chemical formulation of the presented matrices is that they possess a high calcium binding affinity, which is essential for cells differentiation and bone regeneration. Moreover, direct covalent binding and immobilization of a high load of almost any type of biomolecule (enzyme, growth factors, antibody, antigen, antibiotic ...) at their surfaces, is possible. These materials fabricated by electrospinning are synthetic polymers, and most of these products can also be incorporated into the nanofibrous material [42]. As the presented tissues are non-resorbable, longer periods of action of these substances are expected, if compared to some other marketed resorbable materials (from 5 to 15 days) [2,42]. However, whether this membrane adds clinical advantages to existing membranes for guided tissue regeneration remains to be ascertained in future studies.

Table 1. Mean and standard deviations (SD) of tissues' surface roughness, fiber diameter and fiber to fiber distances range.

	Microfiber diameter (microns)	**Nanofiber diameter (nm)**	**Fiber to fiber distances (microns-nm)**	**Surface nanoroughness SRa (nm)**
OH-Matrix	2.05 (0.30) **a**	308.76 (23.73) **A**	8.5 microns to 120 nm	137.07 (21.84) **α**
Ca-Matrix	1.97 (0.18) **a**	312.72 (28.66) **A**	11.5 microns to 110 nm	82.74 (19.64) **β**
Zn-Matrix	2.05 (0.17) **a**	302.40 (19.13) **A**	8 microns to 110 nm	108.40 (16.17) **δ**
Statistics	F=1.24; P=0.29	F=1.39; P=0.25		F= 25.76 P<0.001

Same letter indicates no significant difference ($p<0.05$).

Table 2. Means and standard deviations (SD) of dynamic viscoelastic moduli of tested tissues: complex modulus (*E**), loss modulus (*E*), storage modulus (*E'*) (GPa) and Tan delta (δ).

	Complex Modulus ***E****	**Loss Modulus** ***E***	**Storage Modulus** ***E'***	**Tan delta** **δ**
OH-Matrix	10.03 (4.46) **a**	3.93 (2.04) **A**	6.29 (2.58) **1**	1.07 (0.52) *
Ca-Matrix	13.31 (3.18) **b**	5.29 (2.31) **B**	10.23 (3.03) **2**	0.63 (0.14) +
Zn-Matrix	17.40 (5.36) **c**	6.60 (1.44) **C**	13.29 (5.25) **3**	0.65 (0.15) +
Statistics	F=14.65; P<0.001	F=9.68; P<0.001	F=17.93; P<0.001	F=12.71; P<0.001

Same letter, number or symbol indicate no significant difference ($p<0.05$).

Figure 1

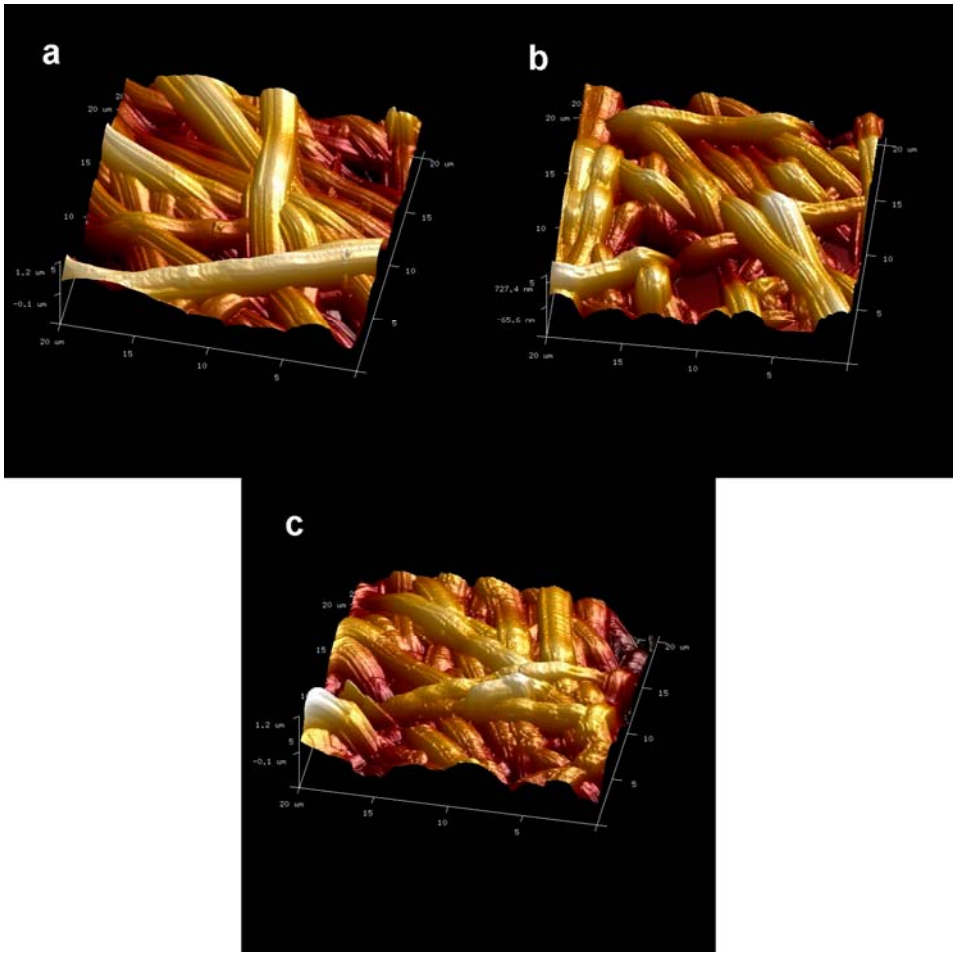

Figure 1. AFM images of the surface's matrices **a)** OH-matrix, **b)** Ca-matrix and **c)** Zn-matrix. Overlapped and randomly distributed nanofibers may be observed. No differences in fiber sizes are encountered between groups, and all surfaces present similar morphology. Spotty nanodeposits are distributed onto the Zn-fibers surfaces.

Figure 2

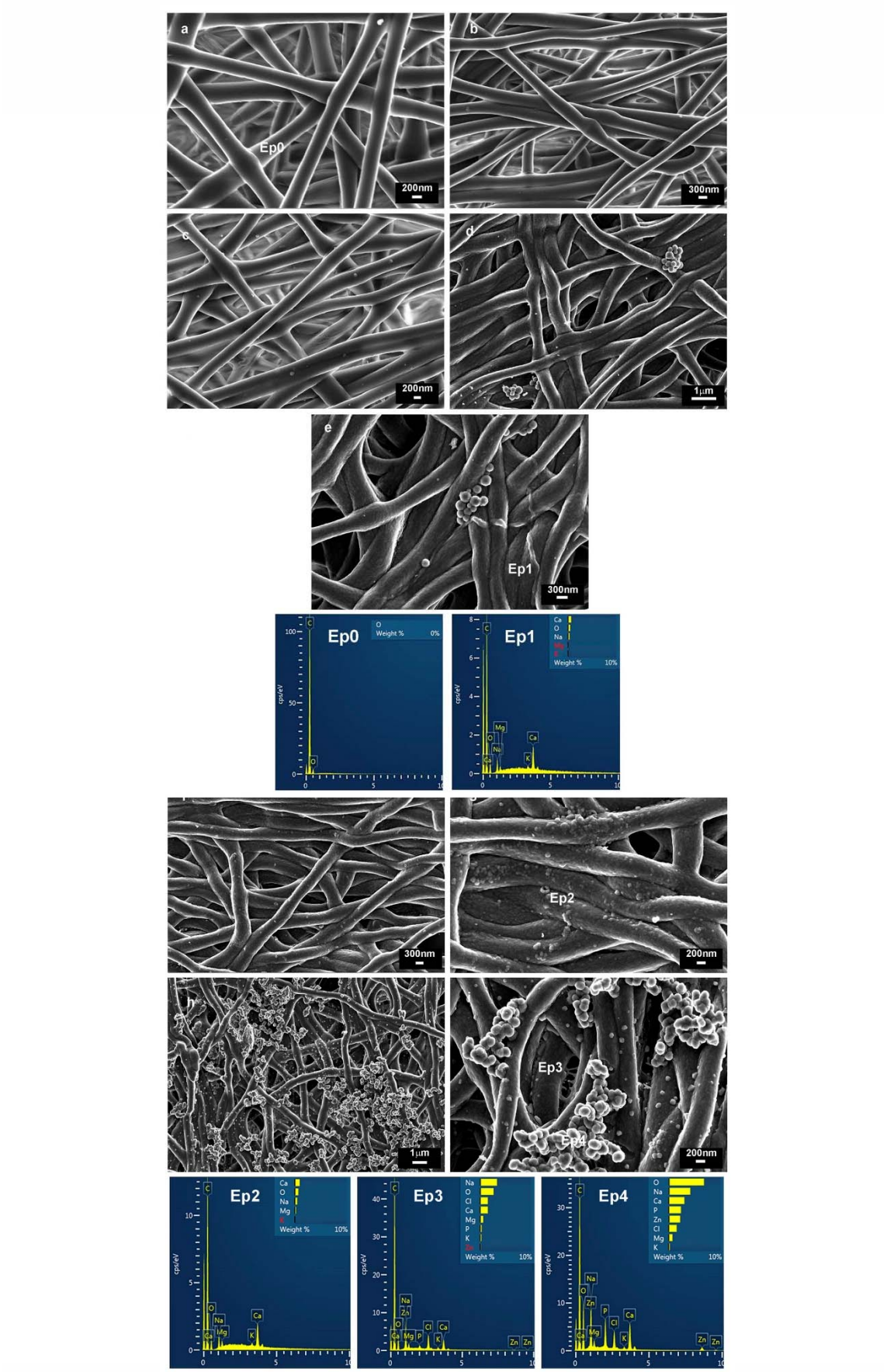
a
Ep0
200nm
b
300nm
c
200nm
d
1μm
e
Ep1
300nm
Ep0
Ep1
300nm
Ep2
200nm
1μm
Ep3
Ep4
200nm
Ep2
Ep3
Ep4

Figure 2: FESEM micrographs of tissues are presented in **a)** OH-matrix. No traces of inorganics elements are shown in the spectra (Ep0). **b)** Ca-matrix and **c)** Zn-matrix. **d)** and **e)** are OH-matrices surface after SBFS immersion for 7 d. Some rounded deposits were observed rarely on the samples. Traces of calcium are found at the EDX spectra (Ep1). **f)** and **g)** are Ca-matrices after immersion in SBFS. Nanofibers increased in diameter about 50 nm and lost their smooth appearance. Spotty calcium deposits were uniformly distributed throughout nanofibers surfaces. Calcium is identified after EDX analysis (Ep2). **h) and i)** correspond to Zn-matrices after immersion in SBFS. Nanofiber diameter is about 500 nm, and fibers lost the smooth appearance of their surface. Nanodeposits of mineral (100 nm) are randomly distributed onto the nanofibers surfaces. Calcium and phosphorous are encountered at the EDX spectra on nanofibers surfaces (Ep3). Numerous agglomerations of other spherical nanocrystals (bigger than 200 nm) are identified onto the Zn-Matrix surface. Calcium, phosphorous and zinc are included at the elemental analysis of these crystal agglomerations (Ep4). At the presented EDX spectra, chloride and sodium are detected after SBFS immersion; magnesium is a contaminant element from the sample holder.

Figure 3

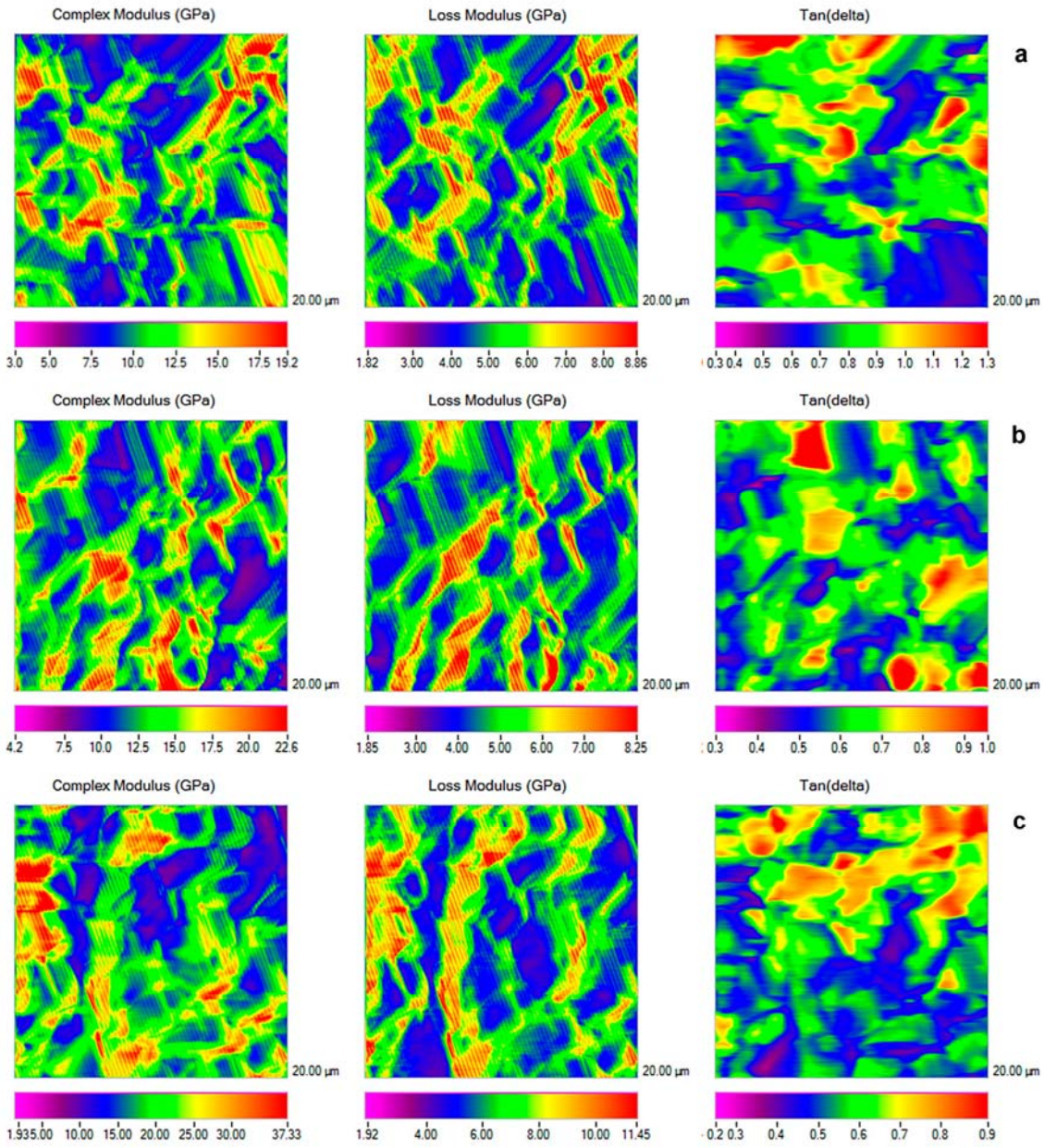

Figure 3. Nano-DMA analysis, on scanning mode, of the surface's matrices **a)** OH-matrix, **b)** Ca-matrix and **c)** Zn-matrix. Properties maps correspond to complex (E^*), loss (E) and storage modulus (E') respectively.

Figure 4

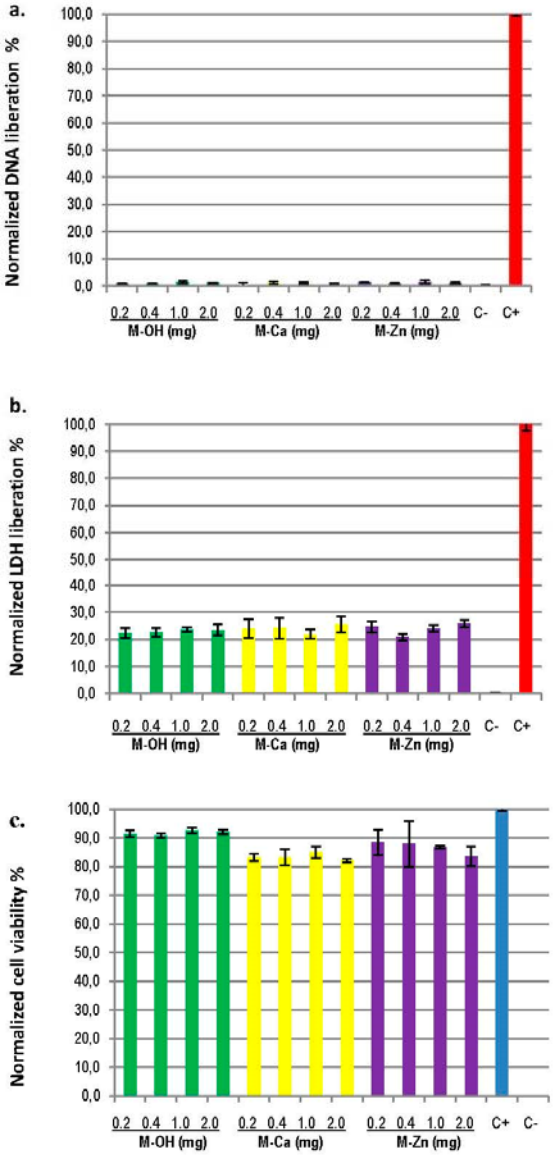

Figure 4. a) Normalized average percentage of DNA liberation of human fibroblasts to the culture medium for the different matrices. Mean values and standard deviations of 3 independent tests for each group are presented. C+ and C– are positive and negative control for cytotoxicity respectively. All the experimental groups were significantly different from controls. Small differences were found between the matrices. **b)** Normalized average percentage of LDH liberation of human fibroblasts to the culture medium for the different groups. Mean values and standard deviations of 5 independent tests for each group are presented. C+ and C– are positive and negative control for cytotoxicity respectively. All the groups are significantly different from controls. No differences are found between the experimental tissues. **c)** Average cell viability according to the Live/Dead assay in human fibroblasts cells incubated with different tissues and controls. Mean values and standard deviations of 5 independent tests for each experimental group are presented. C+ and C– are positive and negative control for cytotoxicity respectively. All the experimental matrices attain cell viability over 80% and are significantly different from controls. Between tested materials small differences are found, Ca-matrices are more cytotoxic than Zn-matrices and both are less cytocompatible than OH-matrices.

Figure 5

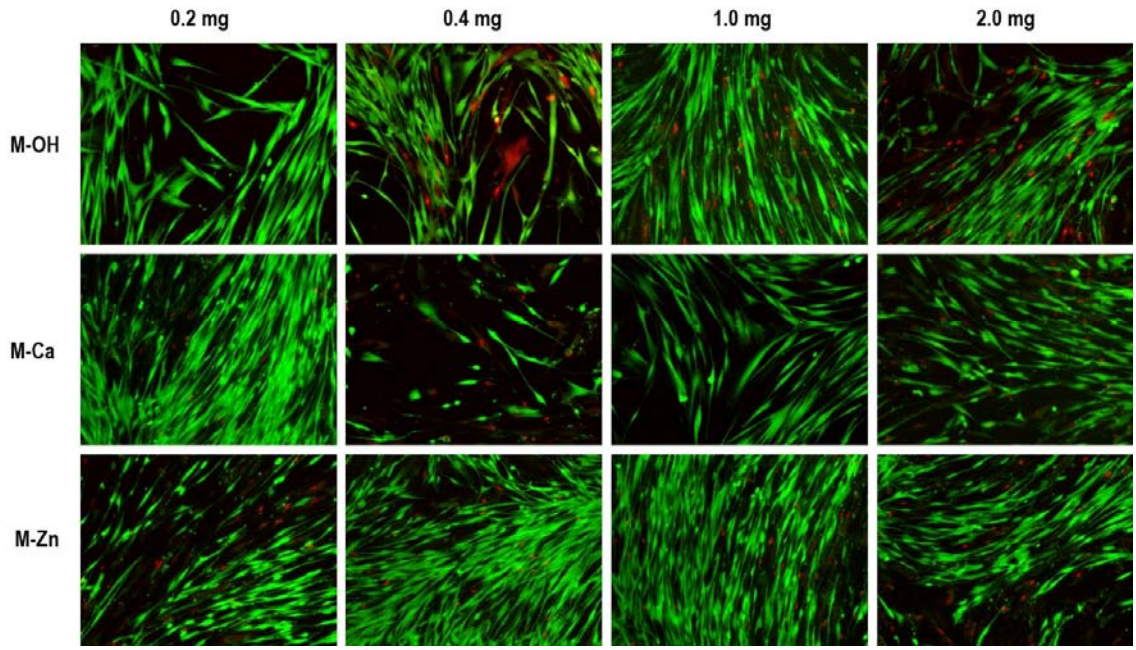

Figure 5: Fluorescence microscopy images corresponding to the analysis of cell viability according to the LIVE/DEAD assay, in human fibroblast cells, incubated with different tissues for 24 h. Green cells correspond to live cells whereas dead cells are stained in red. **a, b, c** and **d** are cells exposed to 0.2, 0.4, 2 and 4 mg of tissues. **e**, **f, g** and **h** correspond to cells exposed to 0.2, 0.4, 2 and 4 mg of calcium loaded tissues. **i, j, k,** and **l** are cells incubated with 0.2, 0.4, 2 and 4 mg of zinc loaded tissues.

COMPLIANCE WITH ETHICAL STANDARDS:

Conflict of Interest: Raquel Osorio declares that she has no conflict of interest. Camilo Andrés Alfonso-Rodríguez declares that he has no conflict of interest. Estrella Osorio declares that she has no conflict of interest. Antonio L. Medina-Castillo declares that he has no conflict of interest. Miguel Alaminos declares that he has no conflict of interest. Manuel Toledano-Osorio declares that he has no conflict of interest. Manuel Toledano declares that he has no conflict of interest.

Funding: Project MAT2014-52036-P supported by the Ministry of Economy and Competitiveness (MINECO) and European Regional Development Fund (FEDER).

Ethical approval: All procedures performed in the present study, involving human participants, were in accordance with the ethical standards of the institutional and/or national research committee and with the 1964 Helsinki declaration and its later amendments or comparable ethical standards. This article does not contain any studies with animals performed by any of the authors.

Informed consent: Informed consent was obtained from all individual participants included in the study.

REFERENCES

1. Ivanovski S, Vaquette C, Gronthos S, Hutmacher DW, Bartold PM (2014) Multiphasic Scaffolds for Periodontal Tissue Engineering. J Dent Res 93(12):1212-1221. doi: 10.1177/0022034514544301.

2. Shimauchi H, Nemoto E, Ishihata H, Shimomura M (2013) Possible functional scaffolds for periodontal regeneration. Japan Dent Sci Rev 49:118-130. doi:10.1016/j.jdsr.2013.05.001.

3. Sam G, Pillai BRM (2014) Evolution of Barrier Membranes in Periodontal Regeneration-Are the third Generation Membranes really here? J of Clin Diagn Res 8: 14-17. doi:10.7860/JCDR/2014/9957.5272.

4. Peng F, Yu X, Wei M. (2011) *In vitro* cell performance on hydroxyapatite particles/poly(L-lactic acid) nanofibrous scaffolds with an excellent particle along nanofiber orientation. Acta Biomater 7: 2585–2592. doi: 10.1016/j.actbio.2011.02.021.

5. Gardin C, Ferroni L, Favero L, Stellini E, Stomaci D, Sivolella S, Bressan E, Zavan B (2012) Nanostructured Biomaterials for Tissue Engineered Bone Tissue Reconstruction. Int J Mol Sci 13: 737-757. doi:10.3390/ijms13010737.

6. Lye KW, Tideman H, Wolke JC, Merkx MA, Chin FK, Jansen JA (2013) Biocompatibility and bone formation with porous modified PMMA in normal and irradiated mandibular tissue. Clin Oral Implants Res 24 Suppl A100:100-109. doi: 10.1111/j.1600-0501.2011.02388.x.

7. Punet X, Mauchauffé R, Rodríguez Cabello JC, Alonso M, Engel E, Mateos-Timoneda MA (2015) Biomolecular functionalization for enhanced cell–material interactions of poly(methyl methacrylate) surface. Regen Biomat 2: 167–175. doi: 10.1093/rb/rbv014.

8. Nandakumar A, Yang L, Habibovic P, van Blitterswijk C (2010) Calcium phosphate coated electrospun fiber matrices as scaffolds for bone tissue engineering. Langmuir 26:7380–7387. doi:10.1021/ la904406b.

9. Seol YJ, Kim KH, Kang YM, Kim IA, Rhee SH (2009) Bioactivity, pre-osteoblastic cell responses, and osteoconductivity evaluations of the electrospun non-woven SiO2-CaO gel fabrics. J Biomed Mater Res B Appl Biomater 90:679–687. doi:10.1002/jbm.b.31334.

10. Münchow EA, Albuquerque MT, Zero B, Kamocki K, Piva E, Gregory RL, Bottino MC (2015) Development and characterization of novel ZnO-loaded electrospun membranes for periodontal regeneration. Dent Mater 31:1038-1051. doi:10.1016/j.dental.2015.06.004.

11. Münchow EA, Pankajakshan D, Albuquerque MT, Kamocki K, Piva E, Gregory RL, Bottino MC (2015) Synthesis and characterization of CaO-loaded electrospun

matrices for bone tissue engineering. Clin Oral Investig Nov 27. doi: 10.1007/s00784-015-1671-5.

12. Osorio E, Toledano M, Aguilera FS, Tay FR, Osorio R (2010) Ethanol wet-bonding technique sensitivity assessed by AFM. J Dent Res 89: 1264-1269. doi: 10.1177/0022034510376403.

13. ISO 23317:2012. Implants for surgery - In vitro evaluation for apatite-forming ability of implant materials.

14. Leonor IB, Balas F, Kawashita M, Reis RL, Kokubo T, Nakamura T (2009) Biomimetic apatite deposition on polymeric microspheres treated with a calcium silicate solution. J Biomed Mater Res B Appl Biomat 91:239-247. doi: 10.1002/jbm.b.31395.

15. Han L, Grodzinsky AJ, Ortiz C (2011) Nanomechanics of the cartilage extracellular matrix. Annu Rev Mater Res 41: 133–168. doi: 10.1146/annurev-matsci-062910-100431.

16. Macosko CW (1994) Rheology: Principles, Measurements, and Applications. VCH, New York, 568pp.

17. Lopez-Lopez MT, Scionti G, Oliveira AC, Duran JD, Campos A, Alaminos M, Rodriguez IA (2015) Generation and Characterization of Novel Magnetic Field-Responsive Biomaterials. PLoS ONE 10: e0133878. doi: 10.1371/journal.pone.0133878.

18. Will J, Detsch R, Boccaccini AR (2013) Structural and biological characterization of scaffolds. Ed. Bandyopadhyay A, Bose S. Elsevier, Oxford: 437 pp.

19. Zhang Y, Zhang X, Shi B, Miron RJ (2013) Membranes for guided tissue and bone regeneration. Annals Oral & Maxillofac Surg 12:10-17.

20. Bružauskaitė I, Bironaitė D, Bagdonas E, Bernotienė E (2016) Scaffolds and cells for tissue regeneration: different scaffold pore sizes-different cell effects. Cytotechnology 68:355-69. doi:10.1007/s10616-015-9895-4.

21. Woo KM, Chen VJ, Ma PX (2003) Nano-fibrous scaffolding architecture selectively enhances protein adsorption contributing to cell attachment. J Biomed Mater Res A 67:531-537. doi:10.1002/jbm.a.10098.

22. Ramon-Marquez T, Medina-Castillo AL, Fernandez-Gutierrez A, Fernandez-Sanchez JF (2016) A novel optical biosensor for direct and selective determination of serotonin in serum by Solid Surface-Room Temperature Phosphorescence. Biosens Bioelectron 82: 217–223. doi: 10.1016/j.bios.2016.04.008.

23. Salehi S, Bahners T, Gutmann JS, Gao SL, Mäder E, Fuchsluger TA (2014) Characterization of structural, mechanical and nano-mechanical properties of electrospun PGS/PCL fibers. RSC Adv 4: 16951. doi: 10.1039/C4RA01237B.

24. Fratzl P (2008) Collagen: Structure and Mechanics. Ed. Fratzl P. Springer US, New York: 131 pp.

25. Polly BJ, Yuya PA, Akhter MP, Recker RR, Turner JA (2012) Intrinsic material properties of trabecular bone by nanoindentation testing of biopsies taken from healthy women before and after menopause. Calcif Tissue Int 90:286-293. doi: 10.1007/s00223-012-9575-8.

26. Xu B, Chow MJ, Zhang Y (2011) Experimental and Modeling Study of Collagen Scaffolds with the Effects of Crosslinking and Fiber Alignment. Int J Biomat 2011:1-12. doi:10.1155/2011/172389.

27. Baker BM, Trappmann B, Wang WY, Sakar MS, Kim IL, Shenoy VB, Burdick JA, Chen CS (2015) Cell-mediated fibre recruitment drives extracellular matrix mechanosensing in engineered fibrillar microenvironments. Nat Mater 14:1262-1268. doi: 10.1038/nmat4444.

28. Baker SR., Banerjee S, Bonin K, Guthold M (2016) Determining the mechanical properties of electrospun poly-ε-caprolactone (PCL) nanofibers using AFM and a novel fiber anchoring technique. Mat Sci Engineer C 59: 203–212. doi: 10.1016/j.msec.2015.09.102.

29. Agrawal R, Nieto A, Chen H, Mora M, Agarwal A (2013) Nanoscale damping characteristics of boron nitride nanotubes and carbon nanotubes reinforced polymer composites. ACS Appl. Mater. Interfaces 27: 12052–12057. doi: 10.1021/am4038678.

30. Espino DM, Shepherd DET, Hukins DWL (2014) Viscoelastic properties of bovine knee joint articular cartilage: dependency on thickness and loading frequency. BMC Musculoskelet Disord 15:205. DOI: 10.1186/1471-2474-15-205

31. Winter HH (1987) Can the gel point of a cross-linking polymer be detected by the $G' - G''$ crossover? Polym Eng Sci 27, 1698-1702. doi: 10.1002/pen.760272209.

32. Pietak AM, Reid JW, Stott MJ, Sayer M (2007) Silicon substitution in the calcium phosphate bioceramics. Biomaterials 28: 4023-4032. doi:10.1016/j.biomaterials.2007.05.003.

33. Chai YC, Carlier A, Bolander J, Roberts SJ, Geris L, Schrooten J, Van Oosterwyck, H, Luyten FP (2012) Current views on calcium phosphate osteogenicity and the translation into effective bone regeneration strategies. Acta Biomaterialia 8:3876-3887. doi: 10.1016/j.actbio.2012.07.002.

34. Tada H, Nemoto E, Kanaya S, Hamaji N, Sato H, Shimauchi H (2010) Elevated extracelular calcium increases expression of bone morphogenetic protein-2 gene via a calcium channel and ERK pathway in human dental pulp cells. Biochem Biophys *Res* Commun 394:1093-1097. doi: 10.1016/j.bbrc.2010.03.

35. Kanaya S, Nemoto E, Sakisaka Y, Shimauchi H (2013) Calcium-mediated increased expression of fibroblast growth factor-2acts through NF-κB and PGE2/EP4 receptor

signaling pathways in cementoblasts. Bone 56:398-405. doi: 10.1016/j.bone.2013.06.031.

36. Riss TL, Moravec RA (2004) Use of multiple assay endpoints to investigate the effects of incubation time, dose of toxin, and plating density in cell-based cytotoxicity assays. ASSAY Drug Develop Technol 2: 51-62. doi:10.1089/154065804322966315.

37. Bock N, Riminucci A, Dionigi C, Russo A, Tampieri A, Landi E, Goranov VA, Marcacci M, Dediu V (2010) A novel route in bone tissue engineering: magnetic biomimetic scaffolds. Acta Biomater 6: 786–796. doi: 10.1016/j.actbio.2009.09.017.

38. Santamaría S, Sanchez S, Sanz M, Garcia-Sanz JA (2016) Comparison of periodontal ligament and gingiva-derived mesenchymal stem cells for regenerative therapies. Clin Oral Invest. doi:10.1007/s00784-016-1867-3.

39. Bottino MC, Arthur RA, Waeiss RA, Kamocki K, Gregson KS, Gregory RL (2014) Biodegradable nanofibrous drug delivery systems: effects of metronidazole and ciprofloxacin on periodontopathogens and commensal oral bacteria. Clin Oral Investig 18:2151-2158. doi: 10.1007/s00784-014-1201-x.

40. Augustine R, Dominic EA, Reju I, Kaimal B, Kalarikkal N, Thomas S (2014) Electrospun polycrapolactone membranes incorporated with ZnO nanoparticles as skin substitutes with enhanced fibroblast proliferation and wound healing. RSC Adv 4:24777–24785. doi: 10.1039/C4RA02450H.

41. Augustine R, Malik HN, Singhal DK, Mukherjee A, Malakar D, Kalarikkal N, Thomas, S (2014) Electrospun polycaprolactone/ZnO nanocomposite membranes as biomaterials with antibacterial and cell adhesion properties. J Polym Res 21:1-17. doi:10.1007/s10965-013-0347-6.

42. Ranjbar-Mohammadi M, Zamani M, Prabhakaran MP, Hajir-Bahrami S, Ramakrishna S (2016) Electrospinning of PLGA/gum tragacanth nanofibers containing tetracycline hydrochloride for periodontal regeneration. Mater Sci Engineer C 58:521-531. doi:10.1016/j.msec.2015.08.066.